

Aeroelastic scaling for rotary-wing aircraft with applications

P.P. Friedmann

Department of Aerospace Engineering, University of Michigan, Ann Arbor, MI 48109-2140, USA

Received 15 October 2003; accepted 25 March 2004

Abstract

This paper presents a new treatment of the aeroelastic scaling problem for rotary-wing vehicles (i.e. helicopters and tiltrotors). It is shown that the offset hinged spring restrained blade model is the rotary-wing equivalent of the typical cross section that has been used during the last 50 years to obtain aeroelastic scaling laws for fixed wing vehicles. A new two-pronged approach for developing refined aeroelastic scaling laws for rotary-wing aeroelastic and aeroservoelastic applications is presented. It combines the classical approach with computer simulations to obtain new refined aeroelastic scaling relations. The rotary-wing scaling laws are applied to the vibration reduction problem in helicopter rotors using an actively controlled, partial span, and trailing edge flap. The results obtained for a Mach scaled rotor are compared with those obtained for a Froude scaled rotor. The results indicate that the Mach scaled rotor is needed so as to obtain the correct actuation requirements for vibration reduction.

© 2004 Elsevier Ltd. All rights reserved.

1. Introduction

The issue of aeroelastic scaling, which has received limited attention during the last two decades has become quite important recently with the increased use of active materials for aeroelastic applications. The area of smart structures, or structures built from active materials, which combine controls, active materials and microprocessors has undergone considerable growth during the last 15 years. Active materials based actuation has been considered and applied to a variety of fixed and rotary-wing problems. The fixed wing applications have focused on static aeroelasticity and divergence control, suppression of panel flutter, wing flutter suppression, and wing/store flutter suppression. The primary rotary-wing applications are vibration reduction and noise suppression in helicopter rotors. Among these applications the most promising are: (1) active flutter suppression in fixed wing aircraft (Lin et al., 1996; Lazarus et al., 1997; Friedmann et al., 1997), and (2) vibration reduction, blade vortex interaction (BVI) alleviation, and noise reduction in rotorcraft (Friedmann, 1998; Fulton and Ormiston, 1998; de Terlizzi and Friedmann, 1999; Chopra, 2000).

Actuators built from adaptive materials that are used for the aeroelastic applications discussed above, are frequently demonstrated on small-scale models used in wind-tunnel tests. The primary purpose of these tests is to demonstrate the feasibility of the proposed approach. It is therefore very important to be able to relate the test results obtained on the small scale model to the behavior of the full scale configuration. In aeroelasticity, such relations between the scale model and the actual configuration are usually governed by aeroelastic scaling laws.

This paper has several objectives: (i) development of basic scaling for rotary-wing aircraft, (ii) implementation of a new two-pronged approach to rotary-wing aeroelastic scaling, which can accommodate both active materials based actuation, as well as active controls and (iii) application of the scaling laws to a rotary-wing application, involving vibration reduction using an actively controlled, partial span, trailing edge flap.

E-mail address: peretzf@umich.edu (P.P. Friedmann).

Nomenclature

a	nondimensional offset between elastic axis (EA) and midchord
a_i	lift curve slope
b	airfoil, or blade, semi-chord
C_{d0}	drag coefficient of blade
C_h, C_l, C_m	hinge moment, lift and pitch moment coefficients per unit span
c_β	nondimensional flap hinge location
$C(k)$	Theodorsen's lift deficiency function
$F_{HX4}, F_{HY4}, F_{HZ4}$	nondimensional 4 rev ⁻¹ hub shears
h, h_0	plunge displacement at the EA, and its initial condition
I_b	blade flapping inertia
I_{EA}	wing section mass moment of inertia about its EA, per unit span
I_f	blade feathering inertia
I_{MB_2}, I_{MB_3}	principal moments of inertia per unit length of blade about cross-sectional axes
I_β	control surface mass moment of inertia about its hinge, per unit span
J_p	cross-sectional polar moment of inertia
k	reduced frequency ($= \omega b / V$)
K_h	spring stiffness in plunge
K_x	spring stiffness in torsion
K_β	control surface torsional stiffness
K_β, K_ζ, K_ϕ	root spring stiffness in flap, lag and torsion, respectively, proportional to blade bending and torsional stiffnesses
L	lift force per unit span
m	section mass per unit span of blade or wing
M	Mach number
M_{EA}	pitch moment per unit span acting at the EA
$M_{HX4}, M_{HY4}, M_{HZ4}$	nondimensional 4 rev ⁻¹ hub moments
M_β, M_ζ, M_ϕ	elastic restoring moments in flap, lag and torsion, respectively
$n_L, n_g, n_v, n_a,$	
n_Ω, n_V, n_ρ	scale factors for length, gravity, speed of rotation, velocity of flight and density
p, \bar{p}	pressure and its nondimensional value ($= p / \frac{1}{2} \rho V^2$)
Q_I, Q_A, Q_D	inertia, aerodynamic and damping moments on blade
r_x	wing section radius of gyration about its EA
r_β	flap radius of gyration about its hinge
R	rotor radius
t, \bar{t}	time and its nondimensional value
$T_1 \dots T_{19}$	coefficients for Theodorsen's theory
V, \bar{V}	free stream velocity and its nondimensional value ($= V / \omega_x b$)
V_F, \bar{V}_F	flutter velocity, and its nondimensional value
$\{x\}$	state vector
x_A	offset between elastic center and aerodynamic center in blade cross section
x_I	offset between elastic center and the mass center in blade cross section
x_x	nondimensional static moment of the airfoil about its EA, for undeflected flap
x_β	nondimensional static moment of the flap about its hinge axis
α	airfoil angle of attack
β	flap deflection angle, also flapping angle of blade
β_p	precone angle
ζ	damping coefficient, also lag angle of blade
θ_f	flap hinge location
Θ_G	blade geometric pitch angle
λ	inflow ratio
μ	advance ratio

μ_m	mass ratio ($= m/\pi\rho b^2$)
ν	kinematic viscosity
ξ	nondimensional plunge displacement ($= h/b$)
ρ	air density
ϕ	blade torsional displacement
ϕ_1, ϕ_2	phase lag angles
ψ	azimuth angle
ω_h	natural frequency in plunge ($= \sqrt{K_h/m}$)
ω_α	natural frequency in pitch ($= \sqrt{K_\alpha/I_{EA}}$)
ω_β	natural frequency of flap ($= \sqrt{K_\beta/I_\beta}$)
$\bar{\omega}_\beta, \bar{\omega}_\xi, \bar{\omega}_\phi$	rotating fundamental blade frequencies in flap, lead-lag and torsion, respectively
Ω	rotor r.p.m.
(*)	nondimensional time derivative $d(\)/d\bar{t}$
(\cdot)	derivatives with respect to time

Such scaling laws are important for the design of small, scaled models, used in rotary-wing aeroelastic and aeroservoelastic testing. These scaling laws play a critical role when interpreting the results of wind tunnel tests involving adaptive materials based actuation for aeroelastic applications. Furthermore, with the advent of a new generation of unmanned rotary-wing vehicles that can vary in size from rotors several feet in diameter to micro air vehicles having rotors as small as six inches or less, which are described in detail in a recent book edited by Mueller (2001), the issue of aeroelastic scaling has resurfaced as an important research topic in a modern context.

2. Background on classical aeroelastic scaling

Classical aeroelastic scaling laws for fixed wing applications have been based on the concept of a typical cross section combined with Theodorsen-type frequency domain aerodynamics (Bisplinghoff et al., 1955). The geometry of this problem is illustrated in Fig. 1. During the last 50 years aeroelastically scaled wind tunnel models have been widely used in testing, and aeroelastic scaling considerations that enable one to relate wind tunnel test results to the behavior of the full scale system have played an important role in aeroelasticity. Such scaling relations have relied on dimensional analysis to establish scaling parameters used for aeroelastically scaled models, suitable for wind tunnel testing. It is interesting to note that despite its importance, the literature on this topic is not extensive, and most of it was done in the late 1950s and early 1960s (Bisplinghoff et al., 1955; Regier, 1963).

Similarity methods in engineering dynamics have been discussed in some specialized books, such as Baker et al. (1991), and mathematical aspects of scaling and self-similarity has been presented recently in a modern setting (Barenblatt, 1996). However, only a very limited amount of this information has been exploited for aeroelastic applications.

Recently, the author has recognized that classical aeroelastic scaling considerations are inadequate when dealing with situations where the control system interacts with the aeroelastic problem, and actuation issues become important. The

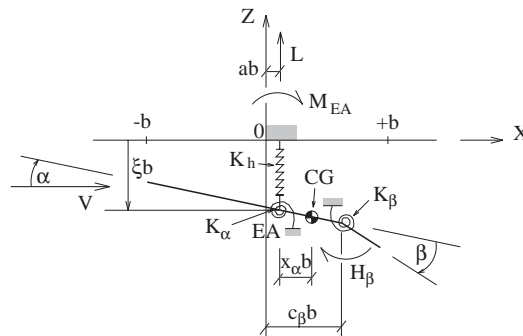


Fig. 1. Definition of parameters for three degree of freedom aeroservoelastic model.

issue of aeroelastic scaling for aeroservoelastic applications, as well as for adaptive materials based actuation has been addressed in recent studies (Friedmann et al., 1997; Friedmann and Presente, 2001).

The classical approach to aeroelastic stability problems, i.e., flutter, for fixed-wing applications is treated in detail in Bisplinghoff et al. (1955). The objective here is to generalize this approach to more general classes of problems. The procedure is best illustrated by considering first the appropriate scaling relations, in incompressible flow, for a two-dimensional airfoil-control surface combination, under the assumption of simple harmonic motion, shown in Fig. 1. The extension of these relations to the compressible case is straightforward. For this case, the equations of motion that describe the typical cross section, with a trailing edge flap and viscous damping is given by

$$[\bar{M}]\{\ddot{q}^*\} + [\bar{C}]\{\dot{q}^*\} + [\bar{K}]\{q\} = \frac{\bar{V}^2}{\pi\mu_m} \begin{Bmatrix} -C_l \\ 2C_m \\ 2C_h \end{Bmatrix}, \quad (1)$$

where the nondimensional time $\bar{t} = \omega_x t$ is used. The damping matrix $[\bar{C}]$ is given by

$$[\bar{C}] = 2 \begin{bmatrix} \frac{\omega_h \zeta}{\omega_x} & 0 & 0 \\ 0 & \zeta & 0 \\ 0 & 0 & \frac{\omega_\beta \zeta}{\omega_x} \end{bmatrix} \quad (2)$$

and the generalized degrees of freedom are

$$\begin{Bmatrix} \zeta(t) \\ \alpha(t) \\ \beta(t) \end{Bmatrix} = \begin{Bmatrix} \zeta_0 e^{i\omega t} \\ \alpha_0 e^{i\omega t + \phi_1} \\ \beta_0 e^{i\omega t + \phi_2} \end{Bmatrix} = \begin{Bmatrix} \zeta_0 e^{i(\omega/\omega_x)\bar{t}} \\ \alpha_0 e^{i[(\omega/\omega_x)\bar{t} + \phi_1]} \\ \beta_0 e^{i[(\omega/\omega_x)\bar{t} + \phi_2]} \end{Bmatrix}. \quad (3)$$

The loads corresponding to Theodorsen's theory (Theodorsen, 1935) are

$$\begin{Bmatrix} -C_l \\ 2C_m \\ 2C_h \end{Bmatrix} = \begin{bmatrix} -\pi & \pi a & T_1 \\ \pi a & -\pi(\frac{1}{8} + a^2) & -2T_{13} \\ T_1 & -2T_{13} & \frac{1}{\pi}T_3 \end{bmatrix} \frac{\{\ddot{q}^*\}}{\bar{V}^2} + \begin{bmatrix} 0 & -\pi & -T_4 \\ 0 & \pi(a - \frac{1}{2}) & -T_{16} \\ 0 & -T_{17} & -\frac{1}{\pi}T_{19} \end{bmatrix} \frac{\{\dot{q}^*\}}{\bar{V}} \\ + \begin{bmatrix} 0 & 0 & 0 \\ 0 & 0 & -T_{15} \\ 0 & 0 & -\frac{1}{\pi}T_{18} \end{bmatrix} \{q\} + C(k) \left(\begin{bmatrix} 0 & -2\pi & -2T_{10} \\ 0 & 2\pi(\frac{1}{2} + a) & 2(\frac{1}{2} + a)T_{10} \\ 0 & -T_{12} & -\frac{T_{10}T_{12}}{\pi} \end{bmatrix} \{q\} \right. \\ \left. + \begin{bmatrix} -2\pi & -2\pi(\frac{1}{2} - a) & -T_{11} \\ 2\pi(\frac{1}{2} + a) & 2\pi(\frac{1}{4} - a^2) & T_{11}(\frac{1}{2} + a) \\ -T_{12} & -T_{12}(\frac{1}{2} - a) & -\frac{T_{11}T_{12}}{2\pi} \end{bmatrix} \frac{\{q^*\}}{\bar{V}} \right). \quad (4)$$

Values of T_1 through T_{14} are defined in Theodorsen (1935), and T_{15} through T_{19} are convenient combinations of the first fourteen T_i s, as indicated in Theodorsen and Garrick (1942). The quantities T_i depend only on the nondimensional hinge location c_β and the nondimensional offset a . Substituting Eqs. (3) and (5) into Eq. (1), neglecting viscous damping effects and dividing by $(\omega/\omega_x)^2$ yields

$$\begin{aligned} & -\zeta_0 - x_\alpha \alpha_0 e^{i\phi_1} - x_\beta \beta_0 e^{i\phi_2} + \left(\frac{\omega_x}{\omega}\right)^2 \left(\frac{\omega_h}{\omega_x}\right)^2 \zeta_0 \\ & = F_1(c_\beta, a, k, \mu_m, \zeta_0, \alpha_0, \phi_1, \beta_0, \phi_2), \\ & -x_\alpha \zeta_0 - r_\alpha^2 \alpha_0 e^{i\phi_1} - (r_\beta^2 + (c_\beta - a)x_\beta) \beta_0 e^{i\phi_2} + r_\alpha^2 \left(\frac{\omega_x}{\omega}\right)^2 \alpha_0 e^{i\phi_1} \\ & = F_2(c_\beta, a, k, \mu_m, \zeta_0, \alpha_0, \phi_1, \beta_0, \phi_2), \\ & -x_\beta \zeta_0 - (r_\beta^2 + (c_\beta - a)x_\beta) \alpha_0 e^{i\phi_1} - r_\beta^2 \beta_0 e^{i\phi_2} + r_\beta^2 \left(\frac{\omega_x}{\omega}\right)^2 \left(\frac{\omega_\beta}{\omega_x}\right)^2 \beta_0 e^{i\phi_2} \\ & = F_3(c_\beta, a, k, \mu_m, \zeta_0, \alpha_0, \phi_1, \beta_0, \phi_2). \end{aligned} \quad (5)$$

Buckingham's π theorem states that the nondimensional solution can then be written in terms of a reduced set of nondimensional combinations that consist of $n - k$ parameters, where n are the original parameters, and $k = 3$ are the primary parameters— M (mass), L (length) and T (time). The nondimensional parameters that can be extracted

from Eqs. (6), using Buckingham’s π theorem are listed below:

$$\xi_0 = \left(\frac{h_0}{b}\right), k = \left(\frac{\omega b}{V}\right), \mu_m = \left(\frac{m}{\pi \rho b^2}\right), \left(\frac{\omega_h}{\omega_z}\right) = \sqrt{\frac{K_h/m}{K_z/I_{EA}} \frac{\omega_\beta}{\omega_z}},$$

$$\frac{\omega_z}{\omega}, r_\alpha^2, r_\beta^2, c_\beta, a, x_z = \left(\frac{S_\alpha}{mb}\right), x_\beta = \left(\frac{S_\beta}{mb}\right), \alpha_0, \beta_0, \phi_1, \phi_2.$$

The first 12 parameters can be expressed as combinations of the three primary variables, while the last four are nondimensional quantities. For aeroelastic stability the quantities of interest are: $\omega_F b / V_F$, ω_F / ω_z and $h_0 / (b \alpha_0)$; where the subscript F refers to the flutter condition. For aeroelastic similarity all other nondimensional parameters such as μ_m , (ω_h / ω_z) , $(\omega_\beta / \omega_z)$, etc. for the model, must have the appropriate values. The external shape (i.e., airfoil type) and Reynolds number also have to be retained. When compressible flow is considered the list of sixteen parameters, given above, has to be augmented by an additional parameter, the Mach number M . Increasing the Mach number modifies the density of the fluid, and with it the mass ratio. Density is related to the Mach number through its value at stagnation:

$$\frac{\rho_0}{\rho} = \left(1 + \frac{\gamma - 1}{2} M^2\right)^{1/(\gamma - 1)}. \tag{6}$$

For the full scale configuration, stagnation density increases with an increase in flight Mach number. The value of the static density remains unchanged and corresponds to the value at the local altitude analyzed. When wind tunnel tests are conducted the value of the stagnation density, related to the value of stagnation temperature and pressure, remains usually unchanged and the value of the static density decreases with an increase in Mach number. When scaling a full size system for wind tunnel tests, the compressibility effect in the tunnel needs to be reflected in the design of a model. For wind tunnels that can utilize gases at higher densities such as the transonic dynamic tunnel (TDT) at NASA Langley research center the special density of the gas used needs to be also considered.

Flutter conditions of similar structural configurations imply that their nondimensional flutter velocity is kept constant, as well as the Mach number. The pitch frequency of a scaled model relates to that of the full scale configuration according to the geometrical scaling ratio:

$$\frac{(\omega_z)_m}{(\omega_z)_w} = \frac{b_w}{b_m}, \tag{7}$$

where subscript m stands for model while subscript w for the prototype.

The scaling of damping properties needs to be also addressed. Eqs. (1) and (2) imply that the damping of each mode is related to the natural frequency associated with that mode. Once the natural frequencies change, the damping coefficient of a corresponding mode needs to be modified to match the appropriate damping loads:

$$\frac{\zeta_m}{\zeta_w} = \frac{(\omega_z)_w}{(\omega_z)_m} = \frac{b_m}{b_w}. \tag{8}$$

The aeroelastic scaling considerations discussed above are based on classical solutions that are obtained from Eqs. (1) and (3)–(6).

3. Refined aeroelastic scaling procedure

For modern applications the classical approach is inadequate for several reasons. The scaling relation for the classical case does not account for the presence of a control system. The control system may experience saturation, free-play and friction which introduce nonlinear effects that can not be represented by the simple linear equations that have been used in this section. Furthermore, the aerodynamic loads may be obtained from computational fluid dynamic codes involving the solutions of the Euler or Navier–Stokes equations, for such cases the aeroelastic model will contain aerodynamic nonlinearities (Friedmann et al., 1997). In such situations the aeroelastic or aeroservoelastic studies are based on refined computer simulations. An alternative, refined, approach to aeroelastic scaling was developed, that is based on a combination of the classical approach and a computer simulation of the specific problem being considered.

Fig. 2 depicts the new two pronged approach aimed at generating refined scaling laws that are applicable to any general linear or nonlinear aeroelastic or aeroservoelastic problem. In this approach basic scaling requirements are established using typical cross-sectional information and dimensional analysis, in a manner that resembles the conventional, or classical, procedure. This process is represented by the left-hand branch in Fig. 2. In parallel, solutions

based on computer simulations are obtained for each aeroelastic or aeroservoelastic problem for which refined scaling laws are required. These computer simulations represent “numerical similarity solutions” that can replace the analytical, closed form, similarity solutions that are usually sought in the framework of mathematical similarity theory (Regier, 1963; Baker et al., 1991). This portion of the procedure is represented by the right-hand branch of Fig. 2. By combining the requirements based on the classical approach with the additional ones based on the computer simulation, a set of expanded or refined aeroelastic scaling requirements is obtained.

These computer simulations enable one to account for additional effects, such as: presence of multiple control surfaces and stores, shock wave motion in transonic flow, saturation, free-play and separation. This approach easily accounts for the presence of the control system, a requirement for aeroservoelastic problems. For such applications the nondimensional frequency variable ω_z/ω is replaced by a nondimensional time variable $\bar{t} = \omega_z t$, and the reduced frequency is replaced by the nondimensional velocity $\bar{V} = V/\omega_z b$. Computer simulations are particularly suitable for examining the intricate scaling requirements governing control power, control forces and hinge moments, which play an important role when extrapolating the model tests to the full scale configuration.

Finally, it is important to note that this approach is particularly suitable for applications that involve the use of adaptive materials based actuation for the modification and control of aeroelastic problems. The two pronged approach can easily account for all the special characteristics and constitutive relations associated with this class of materials (Friedmann and Presente, 2001).

4. Aeroelastic scaling for rotary-wing applications

4.1. Basic rotary-wing scaling problem

The rotary-wing aeroelastic scaling problem has received even less attention than its fixed-wing counterpart. The most comprehensive study in this area is Hunt (1973). A mathematical limitation of this study was the inability to write fundamental, simple equations, comparable to those representing the typical cross section for the fixed-wing problem.

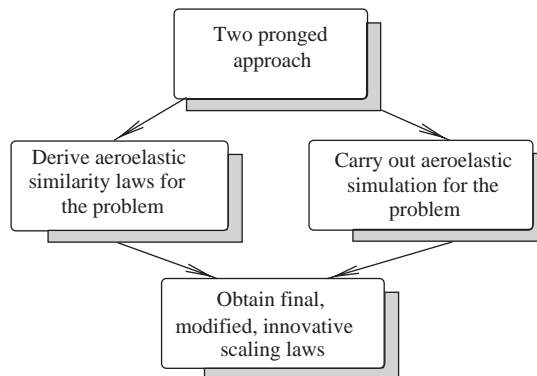


Fig. 2. Two pronged approach for generating refined aeroelastic scaling laws.

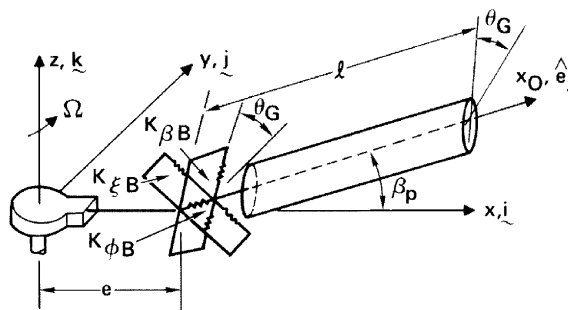


Fig. 3. Offset hinged spring restrained blade model of a hingeless blade.

This limitations has been recently removed (Friedmann, 1998) by recognizing that the rotary-wing equivalent of a typical cross section is the offset hinged, spring restrained model of a helicopter blade shown in Fig. 3.

Using appropriate springs this model, shown in Fig. 3, can be used to represent either an articulated blade or a hingeless blade. The equation of motion for such an offset hinged spring restrained blade can be taken from (Venkatesan and Friedmann, 1984). In Venkatesan and Friedmann (1984) the equations of dynamic equilibrium for the blade configuration shown in Fig. 3, were derived for the fully coupled flap-lag-torsional dynamics of the blade, undergoing moderate deflections, in forward flight. The use of moderate blade deflections, introduces geometrically nonlinear terms in the structural, inertia and aerodynamic terms in the dynamic equations of equilibrium. The aerodynamic loads used in this study (Venkatesan and Friedmann, 1984) were essentially quasi-steady aerodynamic loads corresponding to Greenberg's theory. Note that frequency domain aerodynamics are incompatible with forward flight and therefore the quasisteady assumption is required. Another alternative is the use of time domain aerodynamics, which was employed in Myrtle and Friedmann (2001).

Using the inertia, structural, aerodynamic and damping moments one can write the dynamic equations of equilibrium that can be used as the basis for formulating aeroelastic scaling laws for rotary-wing applications.

The inertia moments found in Venkatesan and Friedmann (1984) are written as

$$\begin{aligned}
 Q_{I_{x3}} = & \frac{m\Omega^2 R^3}{3} [\zeta\ddot{\beta} - \beta\dot{\zeta} + \beta\ddot{\zeta} - 2(\beta\dot{\beta} + \zeta\dot{\zeta})] \\
 & + \Omega^2 \left\{ mx_I \cos \Theta_G \frac{R^2}{2} (\ddot{\beta} - \zeta\phi + \dot{\zeta}\phi) \right. \\
 & + mx_I \sin \Theta_G \frac{R^2}{2} [-\dot{\zeta} + \ddot{\zeta} + 2(\beta\dot{\beta} + \zeta\dot{\zeta}) + \phi\beta] \\
 & + (I_{MB_3} \cos^2 \Theta_G + I_{MB_2} \sin^2 \Theta_G) (-\ddot{\phi} + \ddot{\zeta}\beta + 2\dot{\beta}\dot{\zeta} + \zeta\ddot{\beta} - \ddot{\Theta}_G + \beta\dot{\zeta}) \\
 & \left. + (I_{MB_3} \sin^2 \Theta_G + I_{MB_2} \cos^2 \Theta_G) [\phi - \ddot{\phi} - 2\dot{\beta} + 2\dot{\phi}\dot{\zeta} + 2\phi\dot{\zeta} + 2\zeta\dot{\Theta}_G - \Theta_G] \right\}, \quad (9)
 \end{aligned}$$

$$Q_{I_{y3}} = \frac{m\Omega^2 R^3}{3} (2\dot{\zeta}\beta - \ddot{\beta}), \quad (10)$$

$$Q_{I_{z3}} = \frac{m\Omega^2 R^3}{3} [\zeta - \dot{\zeta} + 2(\zeta\dot{\zeta} + \beta\dot{\beta}) - \zeta(1 + 2\dot{\zeta})]. \quad (11)$$

The elastic restoring moments for an offset hinged spring restrained blade, with no hub and control system flexibility, which is equivalent to a hingeless rotor blade, can be written as (Venkatesan and Friedmann, 1984)

$$M_\beta = (\beta - \phi\zeta)[K_\beta + (K_\zeta - K_\beta) \sin^2 \Theta_G] + (\zeta + \phi\beta)(K_\zeta - K_\beta) \sin \Theta_G \cos \Theta_G, \quad (12)$$

$$M_\zeta = -(\zeta + \phi\beta)[K_\zeta - (K_\zeta - K_\beta) \sin^2 \Theta_G] - (\beta - \phi\zeta)(K_\zeta - K_\beta) \sin \Theta_G \cos \Theta_G, \quad (13)$$

$$M_\phi = -K_\phi(\phi - \zeta\beta). \quad (14)$$

The aerodynamic moments can be written in a general form, that is more compact than the expressions in Venkatesan and Friedmann (1984),

$$Q_{A_{x3}} = \rho a_i b \Omega^2 \frac{R^4}{4} f_{A_{x3}}[\zeta, \beta, \phi, \mu, x_A, \Theta_G, \cos \psi, \sin \psi, \lambda], \quad (15)$$

$$Q_{A_{y3}} = -\rho a_i b \Omega^2 \frac{R^4}{4} f_{A_{y3}}[\zeta, \beta, \phi, \mu, \Theta_G, \cos \psi, \sin \psi, \lambda], \quad (16)$$

$$Q_{A_{z3}} = \rho a_i b \Omega^2 \frac{R^4}{4} f_{A_{z3}} \left[\zeta, \beta, \phi, \mu, \Theta_G, \cos \psi, \sin \psi, \lambda, \frac{C_{d0}}{a_i} \right], \quad (17)$$

where $f_{A_{x3}}$, $f_{A_{y3}}$ and $f_{A_{z3}}$ are complicated expressions given in Venkatesan and Friedmann (1984). The structural damping moments can be expressed as

$$Q_{D_{y3}} = \Omega \dot{\beta} g_{SF}, \quad (18)$$

$$Q_{D_{z3}} = -\Omega \dot{\zeta} g_{SL}, \quad (19)$$

$$Q_{D_{x3}} = -\Omega \dot{\phi} g_{ST}. \quad (20)$$

Note, that when the blade has hinge offset e , and precone β_p the aerodynamic and inertia moments will also depend on these quantities.

The equations of equilibrium of the offset hinged spring restrained blade are given by

$$M_\beta + Q_{I_{y3}} + Q_{A_{y3}} + Q_{D_{y3}} = 0, \quad (21)$$

$$M_\zeta + Q_{I_{z3}} + Q_{A_{z3}} + Q_{D_{z3}} = 0, \quad (22)$$

$$M_\phi + Q_{I_{x3}} + Q_{A_{x3}} + Q_{D_{x3}} = 0. \quad (23)$$

Substituting Eqs. (9)–(20) into Eqs. (21)–(23) yields the dynamic equations of equilibrium for the coupled flap-lag-torsional dynamics of the blade. The resulting dynamic equations of equilibrium are nonlinear, and for aeroelastic stability boundary calculations the equations have to be linearized about a static equilibrium position in hover, or a periodic equilibrium condition in the case of forward flight (Friedmann and Hodges, 1993). These equations can be used as the basis for developing aeroelastic scaling laws in a manner similar to the classical scaling laws described by Eq. (6).

It is convenient to divide Eqs. (21)–(23) by $\Omega^2 I_b$, and introduce nondimensional quantities that are commonly used in helicopter rotor dynamics, such as $\gamma = \text{Lock number} = 2\rho a_i b R^4 / I_b$, where for a uniform blade, one has $I_b = mR^3/3$ and define additional quantities:

$$\frac{K_{\beta B}}{\Omega^2 I_b} = \bar{\omega}_\beta^2, \quad \frac{K_{\zeta B}}{\Omega^2 I_b} = \bar{\omega}_\zeta^2, \quad \frac{K_\phi}{\Omega^2 I_b} = \frac{I_f}{I_b} \bar{\omega}_\phi^2, \quad \frac{\Omega g_{SF}}{I_b \Omega^2} = \eta_{SF} 2\bar{\omega}_\beta,$$

$$\frac{\Omega g_{SL}}{I_b \Omega^2} = \eta_{SL} 2\bar{\omega}_\zeta, \quad \frac{\Omega g_{ST}}{I_b \Omega^2} = \eta_{ST} 2\bar{\omega}_\phi.$$

Rewriting the various parameters affecting the rotary-wing aeroelastic problem in terms of the three basic dimensions M, L, T (mass, length, time) and using dimensional analysis, it can be shown that the problem is governed by several nondimensional parameters, thus

$$\beta, \zeta, \phi \sim F_i \left(M, \text{Re}, \mu, \frac{\bar{\omega}_\beta}{\bar{\omega}_\phi}, \frac{\bar{\omega}_\zeta}{\bar{\omega}_\phi}, \gamma, \frac{x_A}{R}, \frac{x_I}{R}, \frac{V^2}{gR}, \frac{E}{\rho V^2}, \lambda, \frac{C_{d0}}{a_i}, \frac{\omega b}{V}, \Theta_G, \eta_{Si} \right), \quad (24)$$

where the index $i = 1, 2, 3$ implies flap, lag and torsion, respectively.

For complete similarity between dynamic behavior of the model and a full size configuration the function F_i must have the same values in each system, which implies that the nondimensional parameters in F_i must have the same value in both systems. Most of the parameters in Eq. (24) are self-explanatory. A new parameter the *Froude number* = $V^2/(gR)$ appears if gravity loads on the blade are taken into account.

When comparing the parameters in Eq. (24) with those that govern the aeroelastic scaling of fixed wing problem treated in the previous section it is evident that these are more stringent, and satisfying all the relations simultaneously implies constructing a model that has the same dimensions as the full scale configuration.

The common practice in rotary-wing aeroelastic scaling has been to relax these stringent scaling requirements and build either a Mach scaled or Froude scaled model (Friedmann and Hodges, 1993). Furthermore, testing at full scale Re and M numbers is impossible, and usually model rotors are tested at Re numbers that are below full scale values.

4.2. Additional scaling considerations

As indicated earlier, the issue of aeroelastic scaling for rotary-wing applications is one that has not been treated in a systematic manner in the past. However, there are some excellent practical papers that illustrate the state-of-the-art. Straub et al. (1985) presents a detailed description of the design of a dynamically scaled AH-64 main rotor, that was developed for testing on the general rotor model system (GRMS) used in the NASA Langley 4 m × 7 m V/STOL wind tunnel. This was a 27% dynamically scaled model of the AH-64, with a rotor diameter of 13 ft. The primary thrust of the test was performance testing, therefore the following parameters were scaled: M -number, Lock number, stiffness and mass distributions together with blade cross section offsets.

Another recent paper (Singleton and Yeager, 2000) also addresses the issue of important scaling parameters for model-scale rotors. The principal objective of this research was to isolate the effects of Reynolds number, Lock number, and blade elasticity so as to better understand their effect on predicting full scale helicopter rotor performance and dynamic loads from scale-model rotor tests. It was found that both Reynolds and Lock numbers are important, but the role of dynamic scaling was not determined in a definitive manner.

It is useful to systematically identify basic relations that play a useful role in the testing of aeroelastically scale rotors, using Eq. (24). Clearly a fundamental consideration is the geometrical scale of the model defined as

$$n_L = \frac{L_M}{L_V} = \frac{\text{model length}}{\text{full scale vehicle length}}. \quad (25)$$

Certain quantities can be treated as constants, in most cases, such as gravity, viscosity of air and speed of sound in air (Hunt, 1973).

$$n_g = \frac{g_M}{g_{VE}} = n_v = \frac{v_M}{v_{VE}} = n_a = \frac{a_M}{a_{VE}} = 1. \quad (26)$$

In special cases when testing in the transonic dynamic tunnel (TDT) the use of variable density associated with the heavy gas used in the TDT can alleviate partially some of the scaling limitation encountered in constant density tunnels, and therefore for such cases n_v can vary depending on the density ratio. A similar statement also applies to n_a .

If the advance ratio on model and vehicle are the same

$$\frac{n_V}{n_\Omega n_L} = 1$$

or

$$n_\Omega = \frac{n_V}{n_L}. \quad (27)$$

If the Reynolds number is the same for both configurations then $Re = VL\rho/v$ implies

$$\frac{n_V n_L n_\rho}{n_v} = 1,$$

thus

$$n_\rho = \frac{1}{n_V n_L}. \quad (28)$$

If the Mach number, $M = V/a$, is the same on both configurations then

$$\frac{n_V}{n_a} = 1. \quad (29)$$

But Eq. (26) implies $n_a = 1$, thus $n_V = 1$ or the velocity on the model and the vehicle are the same.

If the Froude number is the same, then

$$\frac{n_V^2}{n_g n_L} = 1. \quad (30)$$

But Eq. (26) implies $n_g = 1$ thus

$$n_V = \sqrt{n_L}. \quad (31)$$

Since the Mach number similarity implies $n_V = 1$ while Froude number similarity implies Eq. (31) one has to either have a Mach scaled or a Froude scaled rotor.

Since, in most cases Mach scaling and Froude scaling cannot be simultaneously satisfied, the basic question is which type of scaling should be preferred for a variety of testing objectives. This question can be best answered by a combination of the material provided in the last two sections, combined with the numerical results presented in the next sections, and experimental evidence gleaned from previous tests.

Wind tunnel tests, in general, will have three primary objectives:

- (i) determining aeroelastic stability in hover or forward flight for either: (a) an isolated blade type of configuration, where the fuselage degrees of freedom are locked; or (b) a coupled rotor fuselage system where the fuselage degrees of freedom are free to interact with the blade degrees of freedom;
- (ii) performance testing of flexible rotors, where blade flexibility can affect performance;
- (iii) tests aimed at determining and controlling vibrations levels in forward flight.

First, it is important to emphasize that the refined aeroelastic scaling procedure, described in the previous section, allows one to use computer simulation to augment scaling requirements. Using such simulations it is always possible to compare a Froude scaled rotor with a Mach scaled rotor, for a particular test objective, and the results of the simulation will identify the potential differences between the configurations. If the differences are small then the cost of building the model becomes an important consideration, and then Froude scaling might be more cost effective.

For aeroelastic stability in hover, or coupled rotor/fuselage aeromechanical testing, the static equilibrium position in hover is important (Friedmann and Hodges, 1993) and therefore Froude scaling is more important.

For both performance testing as well as determining and controlling vibration levels in forward flight past experience (Straub et al., 1985; Singleton and Yeager, 2000) suggests that Mach scaling is required. This practical experience is also supported by the numerical results presented in the next section.

Next, it should be noted that the two pronged approach depicted in Fig. 2 applies to rotary-wing aeroelastic scaling just as well as it does to fixed-wing problems.

Finally, it should be noted that Friedmann (1998) and Chopra (2000) contain a description of a number of tests that have been conducted on rotors involving active materials based actuation, for aeroelastic control. As shown (Friedmann, 1998; Chopra, 2000), aeroelastic scaling considerations are sometimes disregarded, and sometimes only partially implemented. Clearly, if scaling considerations are not carefully considered the results obtained may be questionable.

5. Results

The purpose of this section is to illustrate the application of the scaling procedure developed in this paper to the active control of vibrations, implemented by an actively controlled trailing edge flap (ACF), shown in Fig. 4. This approach to controlling vibrations is described in several previous studies (Myrtle and Friedmann, 2001; de Terlizzi and Friedmann, 1999). Vibration reduction in this case is achieved by reducing the 4 rev^{-1} vibratory hub shears and moments, for a typical four-bladed hingeless rotor for which the basic parameters resemble the characteristics of an MBB BO-105 helicopter, for which the basic properties are given in Table 1. Other relevant parameters for this rotor are also given in Myrtle and Friedmann (2001) and de Terlizzi and Friedmann (1999). The various scaling relations for a Mach scaled and Froude scaled rotor are presented in Table 2. These scaling relations are based on the analysis of the offset hinged spring restrained blade presented in the paper, and thus it corresponds to the left-hand branch of Fig. 2.

The computer simulations for the vibration reduction correspond to the right-hand branch of Fig. 2. These simulations provide valuable information on vibration reduction, the flap deflections required for vibration reduction, and the blade tip deflection in the flapwise direction for the baseline case, as well as for the actively controlled case.

Figs. 5–7 depict the 4 rev^{-1} baseline hub shears and moments, together with the controlled hub shears and moments for the Mach scaled and Froude scaled rotors at three different advance ratios: $\mu = 0.15, 0.30$ and 0.40 . The aerodynamic loads on the blade are obtained by combining a time domain compressible unsteady aerodynamic model for the blade flap combination (Myrtle and Friedmann, 2001), combined with a free-wake model (de Terlizzi and Friedmann, 1999) that is capable of representing the basic aspects of blade vortex interaction (BVI) effects. Thus, the loads at $\mu = 0.15$, where BVI effects are important, are higher than at $\mu = 0.30$. However, with increase in advance ratio, the vibratory hub shears and moments increase rapidly. The values plotted in Figs. 5–7 are nondimensionalized hub shears and moments. It is evident from Figs. 5–7 that the principal differences are in the vertical hub shears, however, differences in some of the other components are also evident. Note, that the vertical vibration components play the most important role in vibration reduction studies.

The flap deflections required for the vibration reduction at the three advance ratios are shown in Figs. 8–10. These flap angles are obtained from a combination of 2, 3, 4, and 5 rev^{-1} flap inputs (Myrtle and Friedmann, 2001; de Terlizzi and Friedmann, 1999). As indicated before, $\mu = 0.15$ represents a more challenging vibration reduction task than

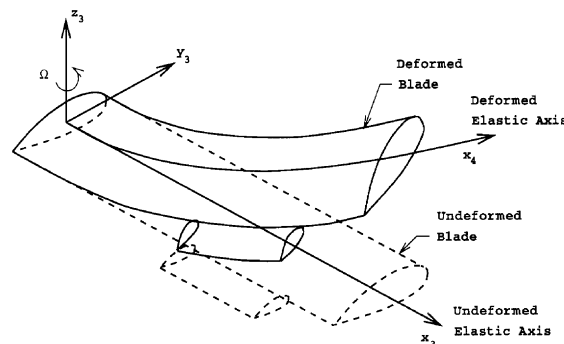


Fig. 4. Blade with actively controlled partial span trailing edge flap.

Table 1
Full scale rotor characteristic parameters based on MBB BO-105

Characteristic parameter	Value	Units
Rotor radius, R	16.11	ft
Rotor angular velocity, Ω	44.51	rad/s
Rotor blade mass per unit length, m	0.1163	lb _f s ² /ft ²

Table 2
Scaling relations

Quantity	Symbol	Mach scaled	Froude scaled
Freestream velocity	n_V	1	$\sqrt{n_L}$
Rotor angular velocity	n_Ω	$1/n_L$	$1/\sqrt{n_L}$
Bending stiffness	n_{EI}	n_L^4	n_L^5
Torsional stiffness	n_{GJ}	n_L^4	n_L^5
Polar moment of inertia	n_{I_p}	n_L^4	n_L^4
Bending moment of inertia	n_{I_b}	n_L^5	n_L^5
Blade mass per unit length	n_m	n_L^2	n_L^2
Young's modulus	n_E	1	n_L
Frequency	n_ω	$1/n_L$	$1/\sqrt{n_L}$
Induced velocity	n_{v_i}	1	$\sqrt{n_L}$
Nondim. speed of sound	$n_{\bar{a}_\infty}$	1	$1/\sqrt{n_L}$
Nondim. accel. of gravity	$n_{\bar{g}}$	$1/n_L$	1

$\mu = 0.30$. The flap angles required in Fig. 8 for the Mach scaled and Froude scaled rotors are quite different. The differences in the flap deflections are much larger than in the vibratory hub loads. The maximum flap angles, for vibration reduction, shown in Fig. 8, are twice as large for the Mach scaled rotor than they were for the Froude scaled rotor. Furthermore, the time history of the deflections is also quite different. These differences between the Mach scaled and Froude scaled rotors diminish when the advance ratio is increased to $\mu = 0.30$ as shown in Fig. 9. Further increase in the advance ratio to $\mu = 0.40$, tends to increase the difference in the magnitude of the maximum flap deflection as well as the time history.

Figs. 11–16 compare the uncontrolled and controlled deflections at the blade tip, in the flapwise direction (i.e., out of the plane of rotation), for the Mach scaled and Froude scaled rotors. It is interesting to note that the differences between the uncontrolled deflections are smaller than the differences between the controlled blade deflections.

It is clear from the results presented in this section that it is essential to use Mach scaled rotors whenever tests for vibration reduction in helicopter rotors are carried out. In particular, the actuation requirements for Mach scaled rotors are substantially higher than for Froude scaled rotors. This is particularly important when designing actuators based on adaptive materials.

6. Concluding remarks

This study re-examines the issue of aeroelastic and aeroservoelastic scaling in the framework of modern aeroelasticity with a particular emphasis on rotary-wing aeroelasticity. This is a very important and somewhat neglected aspect of aeroelasticity. Before presenting the principal conclusions from this study it is important to note that experimental data comparing full scale behavior with behavior measured on scaled rotor is needed. Such data would play a very important role for validating the accuracy of the two pronged approaches for generating refined rotary-wing aeroelastic scaling laws. The principal findings of this study are summarized below.

1. A new, two pronged approach to aeroelastic and aeroservoelastic scaling was developed. It combines the classical approach with computer simulation of the specific problem. It is capable of providing useful scaling information on a large number of quantities that cannot be treated by classical aeroelastic scaling considerations.

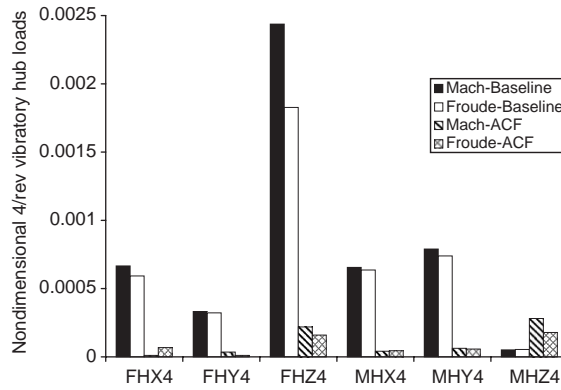


Fig. 5. Comparison of Mach and Froude scaled rotors at $\mu = 0.15$.

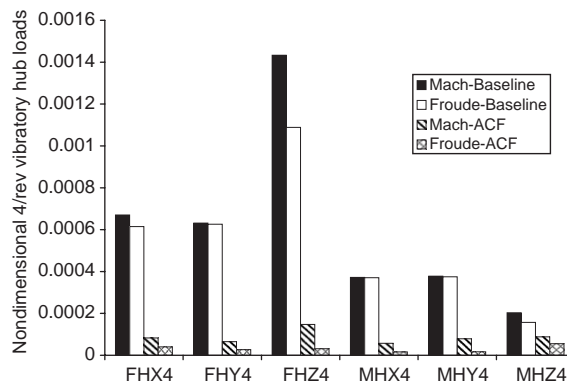


Fig. 6. Comparison of Mach and Froude scaled rotors at $\mu = 0.30$.

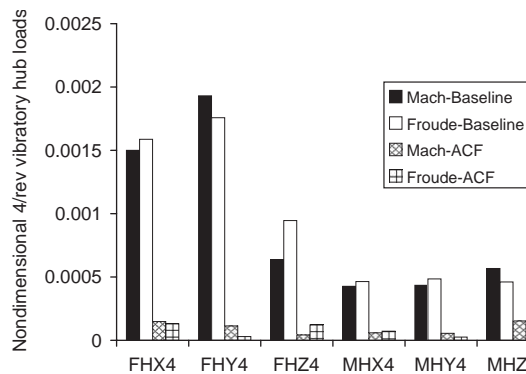


Fig. 7. Comparison of Mach and Froude scaled rotors at $\mu = 0.40$.

2. Numerical simulations of the nondimensional aeroelastic or aeroservoelastic problems provide similarity solutions. Only such solutions predict correctly the behavior of a full scale configuration, as well as that of aeroelastically scaled models. For the rotary-wing problem, such simulations can be carried out for Mach scaled or Froude scaled rotors.
3. The rotary-wing equivalent of the typical cross-sectional analysis used for fixed-wing aeroelastic scaling, is the offset hinged spring restrained blade model. Aeroelastic similarity requirements based on this model indicate that

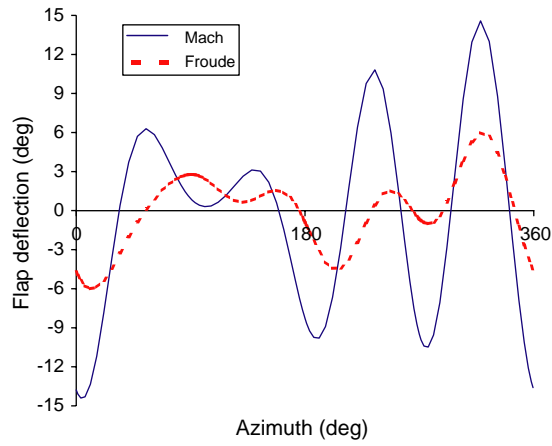


Fig. 8. Comparison of flap deflection for vibration reduction, for Mach and Froude scaled rotors, at $\mu = 0.15$.

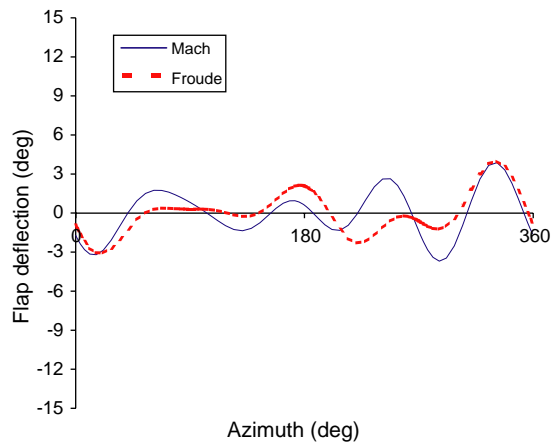


Fig. 9. Comparison of flap deflection for vibration reduction, for Mach and Froude scaled rotors, at $\mu = 0.30$.

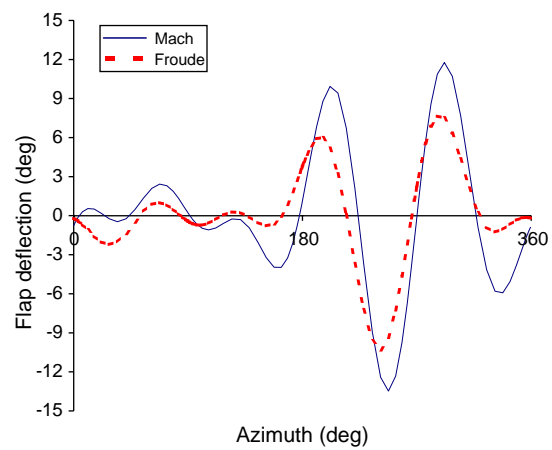


Fig. 10. Comparison of flap deflection for vibration reduction, for Mach and Froude scaled rotors, at $\mu = 0.40$.

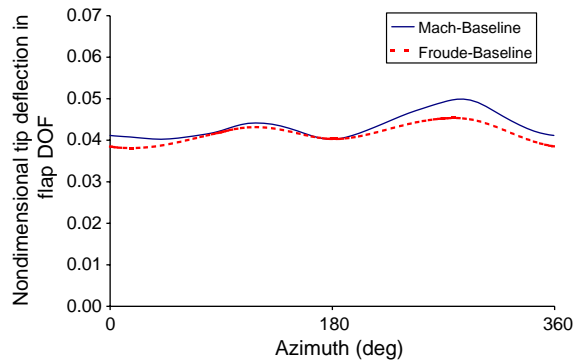


Fig. 11. Comparison of baseline tip deflection, for Mach and Froude scaled rotors, at $\mu = 0.15$.

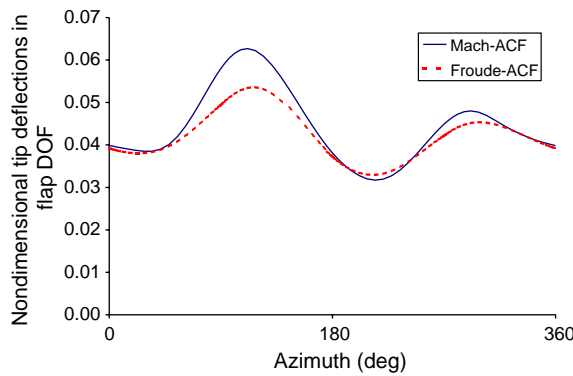


Fig. 12. Comparison of controlled tip deflection, for Mach and Froude scaled rotors, at $\mu = 0.15$.

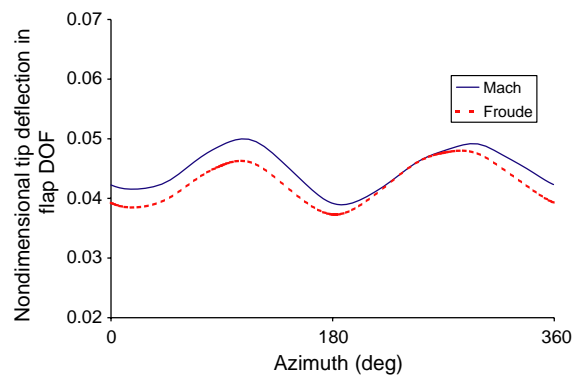


Fig. 13. Comparison of baseline tip deflection, for Mach and Froude scaled rotors, at $\mu = 0.30$.

rotary-wing aeroelastic scaling requirements are more stringent than their fixed-wing counterpart, and these can be satisfied only by full scale configuration.

4. Rotary-wing aeroelastic scaling requirements can be partially satisfied by either Mach scaled rotors, or Froude scaled rotors. Froude scaled rotors are more suitable for aeroelastic stability tests for isolated blades, or coupled

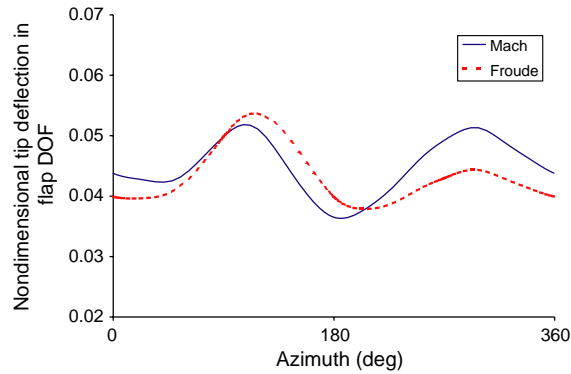


Fig. 14. Comparison of controlled tip deflection, for Mach and Froude scaled rotors, at $\mu = 0.30$.

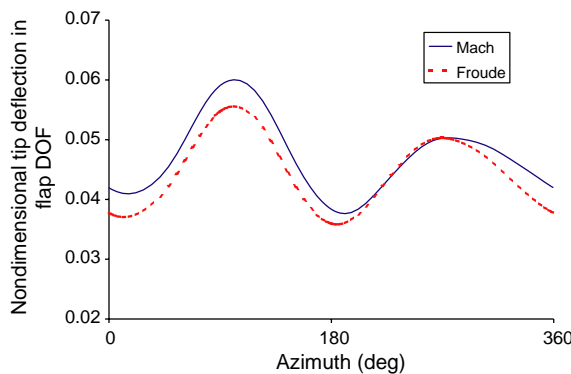


Fig. 15. Comparison of baseline tip deflection, for Mach and Froude scaled rotors, at $\mu = 0.40$.

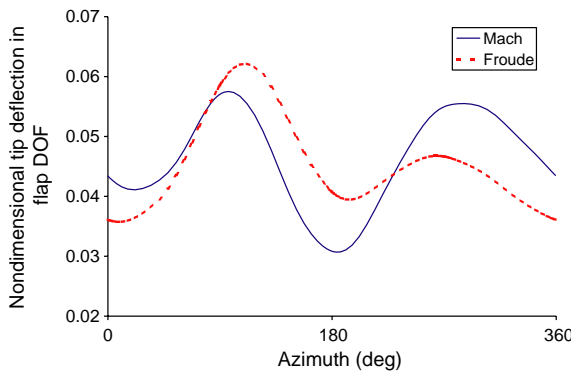


Fig. 16. Comparison of controlled tip deflection, for Mach and Froude scaled rotors, at $\mu = 0.40$.

rotor/fuselage aeromechanical stability test, in hover. For all other test objectives, Mach scaled rotors may be required.

5. The results for the vibration reduction problem on helicopter rotors clearly indicate that Mach scaled rotors have to be used so as to obtain the correct actuation requirements for the actively controlled flap.
6. Aeroelastic scaling considerations have an important role during the testing of scaled models used to determine the characteristics of adaptive materials based actuation.

Acknowledgements

The help of my graduate student, Jack J. McNamara and Li Liu, in generating the numerical results is gratefully acknowledged. The support of the FXB Center for Rotary and Fixed Wing Air Vehicle Design is gratefully acknowledged.

References

- Baker, W.E., Westine, P.S., Dodge, F.T., 1991. *Similarity Methods in Engineering Dynamics: Theory and Practice of Scale Modeling*, Revised Edition. Elsevier, Amsterdam.
- Barenblatt, G.I., 1996. *Scaling, Self-similarity, and Intermediate Asymptotics*. Cambridge University Press, Cambridge.
- Bisplinghoff, R.L., Ashley, H., Halfman, R.L., 1955. *Aeroelasticity*. Addison-Wesley Publishing Co., Cambridge, MA, USA.
- Chopra, I., 2000. Status and application of smart structures technology to rotorcraft systems. *Journal of the American Helicopter Society* 45 (4), 228–252.
- de Terlizzi, M., Friedmann, P.P., 1999. Active control of bvi induced vibrations using a refined aerodynamic model and experimental correlation. In: *Proceedings of the 55th Annual Forum of the American Helicopter Society*, Montreal, Canada, pp. 599–615.
- Friedmann, P.P., 1998. Rotary-wing aeroelastic scaling and its application to adaptive materials based actuation. In: *Proceedings of the 39th AIAA/ASME/AHS/ASC Structures, Structural Dynamics, and Materials Conference and AIAA/ASME Adaptive Structures Forum No. AIAA Paper 98-2698*, Long Beach, CA, USA.
- Friedmann, P.P., Hodges, D.A., 1993. Rotary-wing aeroelasticity with application to vtol vehicles. In: Noor, A.K., Venneri, S.L. (Eds.), *Flight Vehicles, Materials, Structures, and Dynamics-Assessment and Future Directions*, Vol. 5. ASME, New York, pp. 299–391 (Chapter 6).
- Friedmann, P.P., Presente, E., 2001. Active control of flutter in compressible flow and its aeroelastic scaling. *Journal of Guidance, Control and Dynamics* 24 (1), 167–177.
- Friedmann, P.P., Guillot, D., Presente, E., 1997. Adaptive control of aeroelastic instabilities in transonic flow and its scaling. *Journal of Guidance, Control and Dynamics* 20 (6), 1190–1199.
- Fulton, M.V., Ormiston, R.A., 1998. Small-scale rotor experiments with on-blade elevons to reduce blade vibratory loads in forward flight. In: *Proceedings of the 54th Annual Forum of the American Helicopter Society*, Washington, DC, USA, pp. 433–451.
- Hunt, G.K., 1973. Similarity requirements for aeroelastic models of helicopter rotors. CP 1245, Aeronautical Research Council.
- Lazarus, K.B., Crawley, E.F., Lin, C.Y., 1997. Multivariable active lifting surface control using strain actuation: analytical and experimental results. *Journal of Aircraft* 34 (3), 313–321.
- Lin, C.Y., Crawley, E.F., Heeg, J., 1996. Open- and closed-loop results of a strain-actuated active aeroelastic wing. *Journal of Aircraft* 33 (5), 987–994.
- Mueller, T.J. (Ed.), 2001. *Fixed and flapping wing aerodynamics for micro air vehicle applications*. In: *Progress in Astronautics and Aeronautics*, Vol. 195. AIAA, New York.
- Myrtle, T.F., Friedmann, P.P., 2001. Application of a new compressible time domain aerodynamic model to vibration reduction in helicopters using an actively controlled flap. *Journal of the American Helicopter Society* 46 (1), 32–43.
- Regier, A.A., 1963. The use of scaled dynamic models in several aerospace vehicle studies. In: *Proceedings of ASME Colloquium on the Use of Models and Scaling in Simulation of Shock and Vibration*. Philadelphia, PA, ASME, New York, pp. 34–50.
- Singleton, J.D., Yeager, W.T., 2000. Important scaling parameters for testing model-scale helicopter rotors. *Journal of Aircraft* 37 (3), 396–402.
- Straub, F.K., Johnston, R.A., Head, R.E., 1985. Design and development of a dynamically scaled model ah-64 main rotor. *Vertica—the International Journal of Rotorcraft and Powered Lift Aircraft* 9 (2), 165–180.
- Theodorsen, T., 1935. *General theory of aerodynamic instability and the mechanism of flutter*. Technical Report 496, NACA August.
- Theodorsen, T., Garrick, I.E., 1942. *Nonstationary flow about a wing-aileron-tab combination including aerodynamic balance*. Technical Report 736, NACA.
- Venkatesan, C., Friedmann, P.P., 1984. Aeroelastic effects in multi-rotor vehicles with applications to a hybrid heavy lift system, part i: formulation of equations of motion, NASA CR 3822, NASA AMES Research Center, CA, USA.